Hindawi
Shock and Vibration
Volume 2019, Article ID 4178065, 11 pages
https://doi.org/10.1155/2019/4178065

Research Article

Effect of Long-Wavelength Track Irregularities on Vehicle Dynamic Responses

Tao Xin,[1,2] **Pengsong Wang**,[1] **and Yu Ding**[1]

[1]*School of Civil Engineering, Beijing Jiaotong University, Beijing 100044, China*
[2]*Beijing Key Laboratory of Track Engineering, Beijing Jiaotong University, Beijing 100044, China*

Correspondence should be addressed to Tao Xin; xint@bjtu.edu.cn

Received 1 November 2018; Revised 24 January 2019; Accepted 18 February 2019; Published 12 March 2019

Academic Editor: Lutz Auersch

Long-wavelength track irregularities have obvious influence on ride comfort and running stability of high-speed trains. Meanwhile, it brings risk to the inspection of track irregularities since ordinary inspection equipment has difficulties in covering long wavelengths. Previous research on the effect of long-wavelength track irregularities is rare. In order to find the relationship between long-wavelength irregularities and vehicle dynamic responses, a numerical vehicle-track coupling dynamic model based on multibody dynamics and finite element theories is established by using a self-compiling program. One case study is given as an example to show the methodology of determining the sensitive long wavelength and management amplitude of track longitudinal-level irregularities in high-speed railway. The simulation results show that the sensitive long wavelength has a strong correlation with train speed and natural frequency. The simulation and field test results are in good agreement.

1. Introduction

As the main source of vehicle's vibration, track irregularities obviously affect ride comfort and running safety [1–5]. Track irregularities can be divided into long-wavelength and short-wavelength irregularities. Short-wavelength irregularities generally cause noise and vibration in railway trains and environment. Long-wavelength irregularities will give rise to low-frequency oscillations of trains [6]. Because the natural frequency of railway trains is usually around 1 Hz [7], a resonance phenomenon may occur due to long-wavelength irregularities. Meanwhile, long-wavelength irregularities also bring risk to the inspection of track irregularities because ordinary inspection equipment has difficulties in covering them. To ensure the running safety of trains and to enhance the maintenance of tracks, it is necessary to study the relationship between long-wavelength irregularities and dynamic responses of high-speed trains.

As an important interference source of railway vibrations, track irregularities have been studied by many researchers all over the world. Hung and Hsu [6] investigated the relationship between train speed, track irregularities, vibration level of carbody, and bridge using three-dimensional finite element transient dynamic analysis and studied the influence of different parameters on vehicle vibration. A pattern was proposed to avoid resonance. Yang et al. [8] analysed the effect of random track irregularities and train speeds on the system responses under moving vehicle loads using dynamic simulation. Xu et al. [9] solved the probabilistic transmission problem between track irregularity sets and vehicle's responses based on the finite element method and dynamic equilibrium equations. Ling et al. [10] applied a three-dimensional model to investigate four typical types of track irregularities' influence on dynamic responses of a tram vehicle. The results showed that dynamic responses of tram vehicles were significantly influenced by the wavelength characteristics of track defects. Sadeghi et al. [11] investigated the accuracy and effectiveness of two-dimensional and three-dimensional numerical models in predicting the influence of track irregularities on wheel/rail dynamic force. The results indicated that a three-dimensional model is necessary for the prediction of wheel/rail interaction because there were limitations for the two-dimensional model. Nokhbatolfoghahai et al. [12] presented

a dynamic model to investigate the influence of random irregularities on the vibration of tank trains. Based on the numerical model, the natural frequency, frequency response functions, and spectrum densities were calculated. Xu et al. [13] developed a united model to investigate the wheel/rail force induced by track irregularities at middle-low frequencies. To reflect the time-frequency characteristics of track irregularities, the wavelet transform and Wigner–Ville distribution method were combined in the model.

Some research work based on measurements has also been done. Czop et al. [14] presented an approach for the detection of track irregularities based on the measurements of bearing box acceleration during the operation of vehicles. Fujimoto et al. [15] studied the carbody vibration of a Shinkansen train excited by the track alignment irregularities through the comparison between measurements and numerical simulation. Gullers et al. [16] selected ten stretches of a Swedish track to inspect rail irregularities and confirmed the correlation between corrugation and wheel/rail dynamic force. Karis et al. [17] used the filtered data measured from Swedish research and EU projects to evaluate track irregularities' influence on dynamic responses of vehicles. Haigermoser et al. [18] presented a detailed overview of track irregularities and summarized its measurement, assessment, and simulation methods. Li et al. [19] proposed a new mobile approach to measure track irregularities using a laser-aided inertial navigation system (INS).

Among the published research results, there are few studies on the effect of long-wavelength irregularities and management scope of sensitive wavelength in high-speed railway. Moreover, the research on long-wavelength track irregularities is mostly from the aspect of vehicle dynamics, and the influence of the track is rarely considered. An ordinary vehicle-track coupling model is usually not able to simulate the effect of long-wavelength irregularities because of model size and computing cost. In this paper, a self-compiling program is adopted to establish the vehicle-track coupling model. CRTS III ballastless track widely used in China high-speed railway is taken into account. Through the model, sensitive long wavelength and management amplitude are analysed and one regression formula is proposed for the inspection and management of track geometry.

The organization of this paper is as follows. Section 2 presents a numerical analysis model. Section 3 analyses the dynamic responses caused by long-wavelength track irregularities and a detailed case study is presented to show the methodology of determining the sensitive long wavelength and management amplitude. The concluding remarks are presented in Section 4 together with the findings and suggestions.

2. Numerical Model

The system model consists of a vehicle model, track model, and wheel/rail interaction model. The vehicle model and track model are established based on multibody dynamics and finite element theories, respectively. The vehicle model and track model are rigid-flexible coupled through the wheel/rail interaction model with track irregularities included.

2.1. Vehicle Model. A classic 4-axle railway vehicle is presented as an example to illustrate the vehicle modelling method, as shown in Figure 1. The vehicle consists of one carbody, two bogie frames, and four wheel-sets which are regarded as rigid components were connected by spring-damper elements with each other, neglecting their elastic deformation during vibration.

The vehicle model contains 31 degrees of freedom. 5 degrees of freedom in lateral, vertical, rolling, pitching, and yawing directions are considered for the carbody and two bogie frames. The pitch vibration of each wheel-set is not considered. The wheel profile named LMA which is widely adopted in China high-speed railway is shown in Figure 2.

2.2. Track Model. The track model is composed of rails, slabs, and fasteners. Two parallel rails are modelled as two continuous beams supported on a discrete-elastic foundation. The rail profile named CHN60 is shown in Figure 3. The rail cant is 1/40. The deformation of each beam element is defined by the degree of freedom at the end nodes i and j. The displacement vector $\boldsymbol{\delta}_b^e$ of the beam is shown in the following equation:

$$\boldsymbol{\delta}_b^e = \left[u_i, \theta_i, u_j, \theta_j\right]^T, \tag{1}$$

where u_i and u_j are the translational displacements of nodes i and j and θ_i and θ_j are the rotational displacements of nodes i and j. The rails are represented by the beam elements in Figure 4(a). The slab tracks composed of the track slabs, self-compacting concrete slabs, and base slabs are modelled as solid elements with 8 nodes (Figure 4(b)). Each node has 3 degrees of freedom in longitudinal, lateral, and vertical directions, respectively. The rail and slab are connected by several fasteners which are simplified as the spring-damper elements (Figure 4(c)).

2.3. Wheel/Rail Interaction Model. The interaction between vehicle and track is carried out by wheel/rail contact as shown in Figure 5 [20]. The equivalent conicity is shown in Figure 6. The normal forces of the wheel/rail contact are calculated by Hertz contact theory and the tangential forces are calculated based on Kalker linear theory. Track irregularities are considered in the calculation of wheel/rail contact geometry parameters.

Generally, track irregularities can be classified into four different geometric deviations: track longitudinal level, track alignment, track gauge, and track cross level. The longitudinal level and track alignment irregularities under various running speeds are selected as examples for demonstrating the relationship between long-wavelength irregularities and dynamic responses of vehicles. Since actual track irregularities have irregular wave shapes which can be decomposed into various harmonic waves with different frequencies and amplitudes through Fourier transform, the track irregularities with basic sinusoidal waves are taken into account in the model. The schematic diagrams of longitudinal level and alignment irregularities are shown in Figure 7(a) and Figure 7(b), respectively.

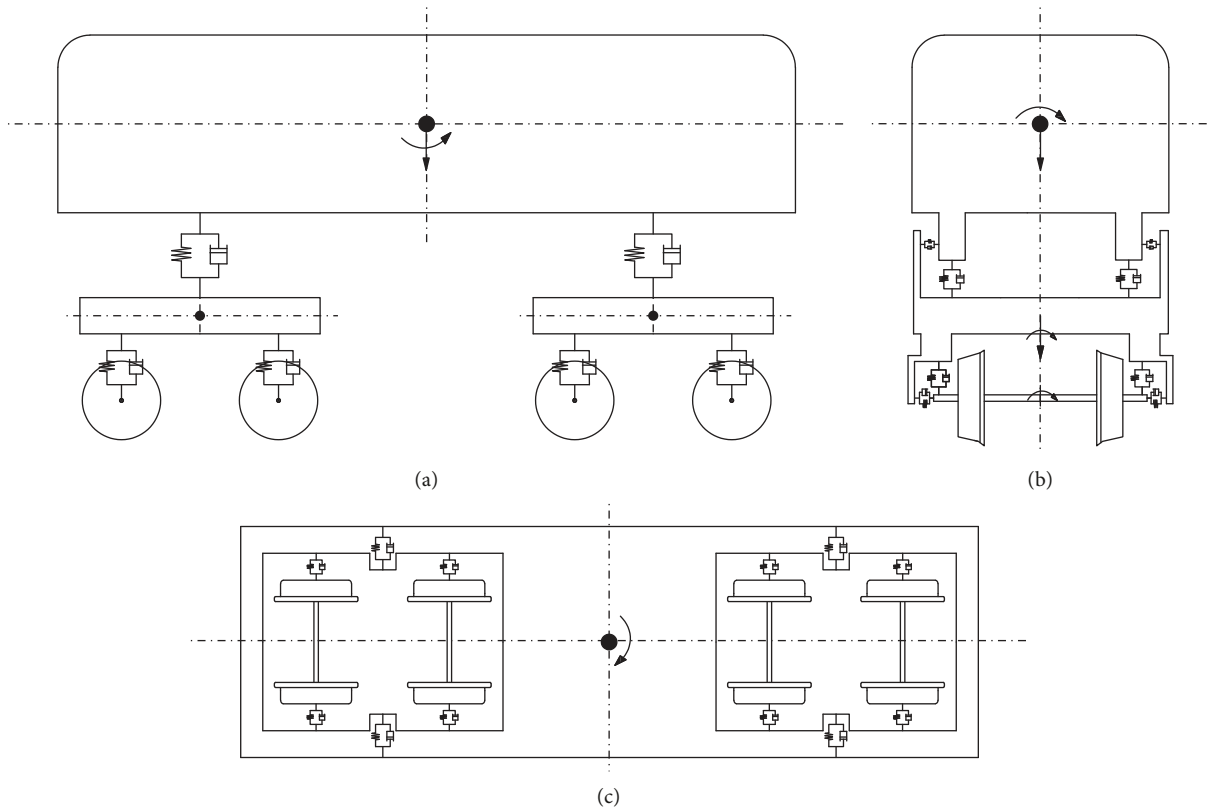

Figure 1: Vehicle model. (a) Front view. (b) Left view. (c) Bottom view.

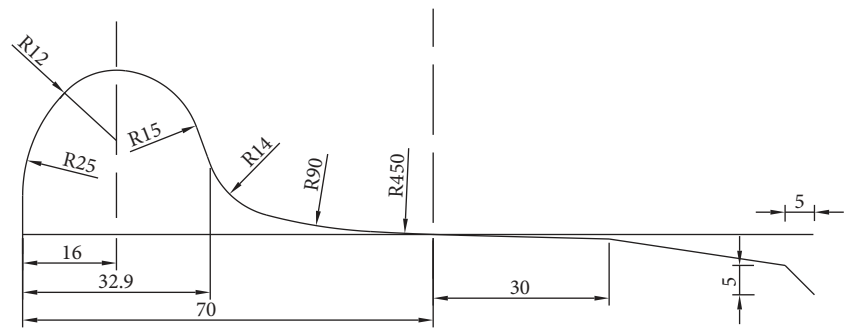

Figure 2: Wheel profile.

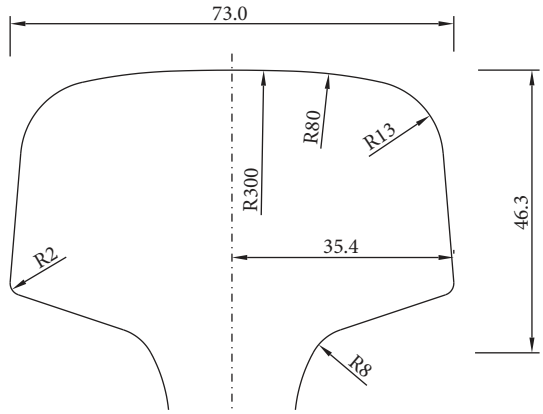

Figure 3: Rail profile.

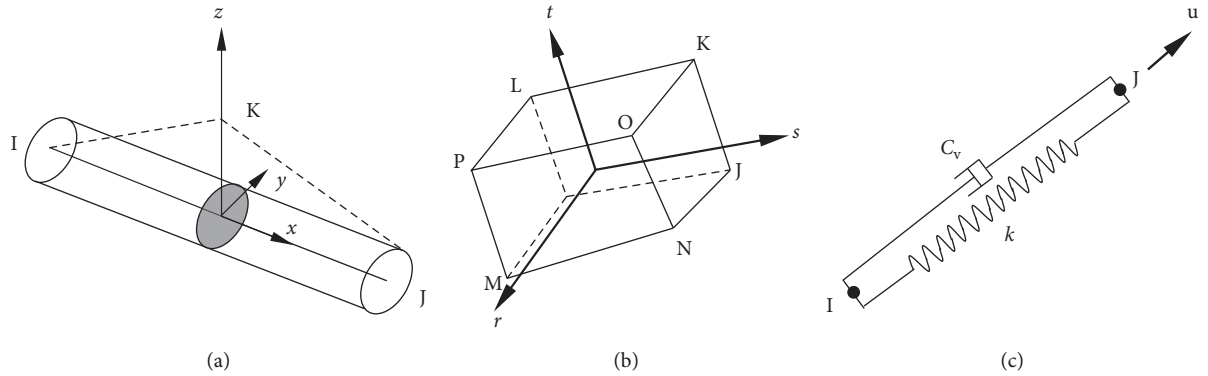

Figure 4: Track model. (a) Beam element. (b) Solid element. (c) Spring-damper element.

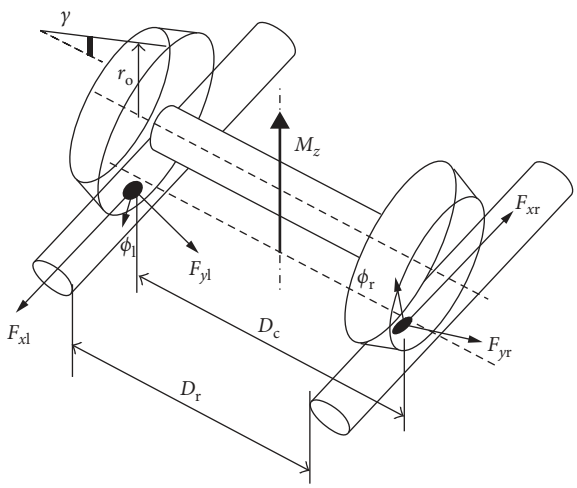

Figure 5: Schematic diagram of wheel rail contact.

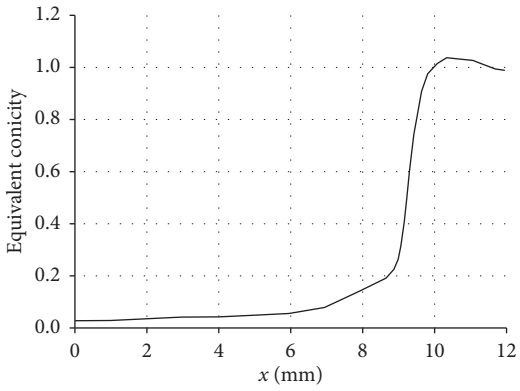

Figure 6: Equivalent conicity.

A sinusoidal irregularity is expressed as follows:

$$y = \eta \sin \frac{2\pi x}{\lambda}, \tag{2}$$

where λ and η are the wavelength and amplitude, respectively.

The maximum wavelength of track irregularities in the model is 200 m. For the stability of numerical calculation, 10 wavelengths are used for model input. A self-compiling method is adopted to enhance the computing efficiency instead of using commercial software and package.

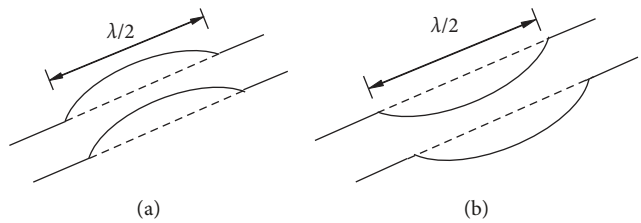

Figure 7: Track irregularities. (a) Longitudinal level. (b) Track alignment.

2.4. Vibration Equation. The vibration equation for the vehicle-track coupled system is expressed as follows:

$$\begin{bmatrix} \mathbf{M}_{vv} & \mathbf{0} \\ \mathbf{0} & \mathbf{M}_{tt} \end{bmatrix} \begin{Bmatrix} \ddot{\delta}_v \\ \ddot{\delta}_t \end{Bmatrix} + \begin{bmatrix} \mathbf{C}_{vv} & \mathbf{C}_{vt} \\ \mathbf{C}_{tv} & \mathbf{C}_{tt} \end{bmatrix} \begin{Bmatrix} \dot{\boldsymbol{\delta}}_v \\ \dot{\boldsymbol{\delta}}_t \end{Bmatrix} + \begin{bmatrix} \mathbf{K}_{vv} & \mathbf{K}_{vt} \\ \mathbf{K}_{tv} & \mathbf{K}_{tt} \end{bmatrix} \begin{Bmatrix} \boldsymbol{\delta}_v \\ \boldsymbol{\delta}_t \end{Bmatrix} = \begin{Bmatrix} \mathbf{P}_v \\ \mathbf{P}_t \end{Bmatrix}, \tag{3}$$

where **M**, **C**, and **K** represent the mass, damping, and stiffness matrixes of the whole model. $\boldsymbol{\delta}$, $\dot{\boldsymbol{\delta}}$, and $\ddot{\boldsymbol{\delta}}$ represent the displacement, velocity, and acceleration vectors. **P** represents the load vector. The subscripts t and v represent the track and vehicle. The equation is solved by the Newmark-β integration method.

According to the modelling method discussed in the earlier sections, a numerical vehicle-track system dynamics model (VTSDM) by a self-compiling program is completed (Figure 8).

2.5. Model Parameters. CRH380 is the newest high-speed train with a maximum operating speed of 380 km/h in China. CRTS III is a self-developed track system widely used in Chinese high-speed railway. Main parameters of CRH380 and CRTS III are adopted by the model. They are listed in Tables 1 and 2, respectively.

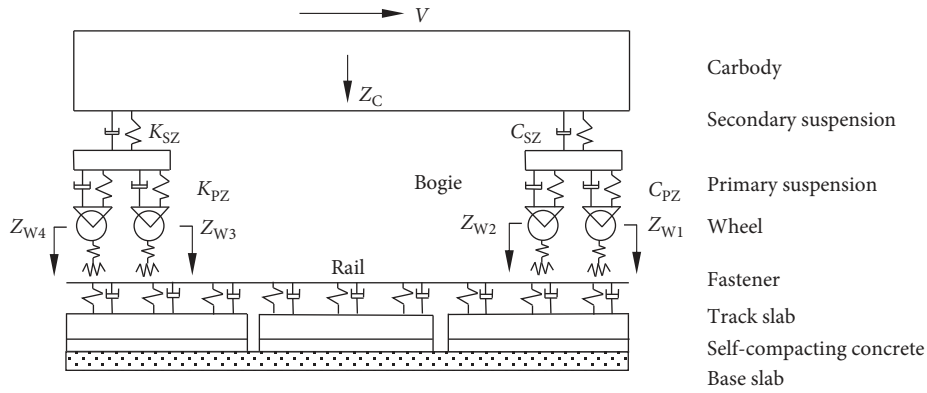

Figure 8: Schematic diagram of the VTSDM model.

Table 1: Vehicle parameters.

Parameters	Notation	Value
Mass of carbody	m_c (kg)	40000
Mass of bogie frame	m_b (kg)	3200
Mass of wheel-set	m_w (kg)	2400
Moment of inertia of carbody frame about x axis	I_{cx} (kg·m^2)	1840000
Moment of inertia of carbody frame about y axis	I_{cy} (kg·m^2)	547000
Moment of inertia of carbody frame about z axis	I_{cz} (kg·m^2)	1920000
Moment of inertia of bogie frame about x axis	I_{bx} (kg·m^2)	3200
Moment of inertia of bogie frame about y axis	I_{by} (kg·m^2)	6800
Moment of inertia of bogie frame about z axis	I_{bz} (kg·m^2)	7300
Moment of inertia of wheel-set about x axis	I_{wx} (kg·m^2)	1210
Moment of inertia of wheel-set about y axis	I_{wy} (kg·m^2)	1210
Lateral stiffness of primary suspension	K_{1y} (MN/m)	3.0
Vertical stiffness of primary suspension	K_{1z} (MN/m)	1.04
Lateral stiffness of secondary suspension	K_{2y} (MN/m)	0.24
Vertical stiffness of secondary suspension	K_{2z} (MN/m)	0.40
Lateral damping of primary suspension	C_{1y} (kN·s/m)	0.0
Vertical damping of primary suspension	C_{1z} (kN·s/m)	5.0
Lateral damping of secondary suspension	C_{2y} (kN·s/m)	30.0
Vertical damping of secondary suspension	C_{2z} (kN·s/m)	6.0
Half distance between primary suspension systems	d_1 (m)	0.748
Half distance between secondary suspension systems	d_2 (m)	0.978
Radius of wheel	R_w (m)	0.457
Distance between carbody and second suspension system	h_1 (m)	1.70
Distance between secondary suspension system and bogie	h_2 (m)	0.14
Distance between primary suspension system and bogie	h_3 (m)	0.28
Distance between two bogies	d_b (m)	17.375
Distance between wheel-sets	d_w (m)	2.5

Table 2: Track parameters.

Parameters	Notation	Value
Mass of rail beam per unit length	m_r (kg)	60.64
Area of rail section	A_r (cm^2)	77.45
Elastic modulus of rail	E_r (MPa)	205900
Rail moment of inertia about z axis	I_{rz} (cm^4)	3217
Fastener stiffness	K_p (MN/m)	60.0
Fastener damping	C_p (kN·s/m)	27.0
Width of track slab	b_1 (m)	2.5
Thickness of track slab	t_1 (m)	0.21
Width of self-compacting concrete	b_2 (m)	2.5
Thickness of self-compacting concrete	t_2 (m)	0.1
Width of concrete base slab	b_3 (m)	3.1
Thickness of concrete base slab	t_3 (m)	0.3

3. Results and Discussion

The dynamic responses of high-speed vehicles induced by long-wavelength track irregularities are simulated based on VTSDM. Because the natural frequency of railway trains is usually around 1 Hz and the ride comfort is related to sensitive long wavelength of track irregularities, the acceleration in the center of carbody is selected as an indicator to determine the sensitive wavelength values.

Multiple sinusoidal waves are adopted in the numerical simulation. For example, the longitudinal-level irregularity with 10 waves is shown in Figure 9(a). The corresponding simulation result is shown in Figure 9(b). It can be seen that the acceleration becomes stable after five fluctuations. The

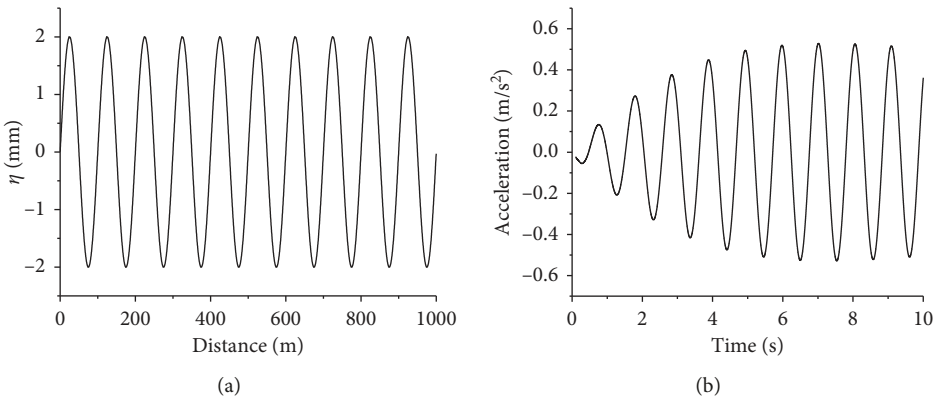

Figure 9: Simulation input and output. (a) Sinusoidal longitudinal-level irregularity. (b) Simulation result.

maximum values of dynamic responses at a steady state are recorded for further analysis.

3.1. Sensitive Long Wavelength. To study the relationship between track irregularity wavelength and vehicle acceleration, the wavelength varies from 70 m to 200 m by increment step 10 m and the amplitude is set as constant. Train speed is 350 km/h. The vertical acceleration induced by the longitudinal-level irregularities is shown in Figure 10(a), and the lateral acceleration induced by track alignment irregularities is shown in Figure 10(b).

It can be seen that the sensitive long wavelength of longitudinal-level irregularities is 110 m and the sensitive long wavelength of track alignment irregularities is 150 m. As we all know, a wheel running with speed v over a sinusoidal rail irregularity of wavelength λ will perceive an excitation frequency f which can be represented as follows:

$$f = \frac{v}{\lambda}. \tag{4}$$

To investigate the relationship between excitation frequencies and natural frequencies of vehicles, a modal analysis is carried out to calculate the natural frequency. The vertical natural frequency is 0.92 Hz, and the lateral natural frequency is 0.85 Hz. Generally, when the excitation frequencies are close to the natural frequencies of vehicles, resonance phenomenon will occur.

With a train speed $v = 350$ km/h, the sensitive long wavelength of longitudinal irregularities $\lambda_s = 110$ m. The corresponding excitation frequency $f = (350/3.6)/110 = 0.92$ Hz. The result is the same as the calculated vertical natural frequency. Therefore, the sensitive long wavelength of the longitudinal irregularity λ_s can be expressed as follows:

$$\lambda_s = \frac{v}{f_0}, \tag{5}$$

where f_0 is the vehicle's vertical natural frequency.

It can be seen that the sensitive long wavelength of track alignment irregularities is 150 m. Correspondingly, the excitation frequency is 0.65 Hz, while the calculated lateral natural frequency is 0.85 Hz. The result from modal analysis is higher than that calculated from vehicle-track dynamic simulation. Thus, the sensitive long wavelength of track alignment irregularities cannot be estimated directly from equation (5) in this case. This is because the lateral track irregularities' excitation may cause moderate vertical vibration simultaneously to generate the vertical-lateral-coupled vibration phenomenon which is not purely lateral vibration.

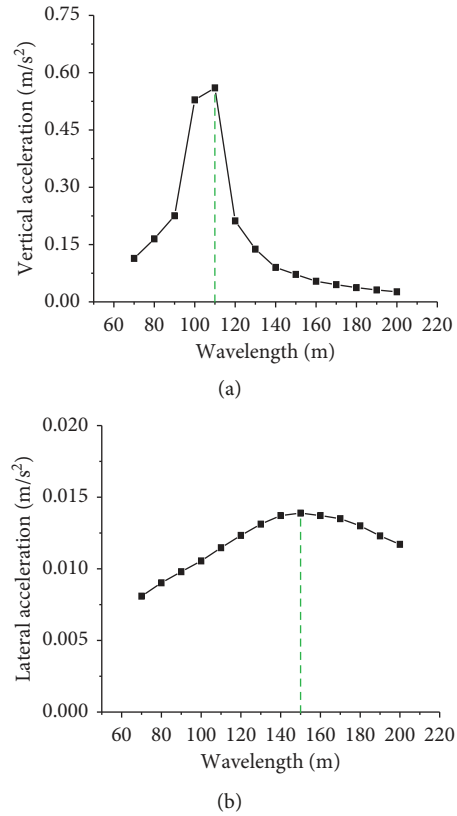

Figure 10: Vehicle dynamic responses. (a) Vertical acceleration. (b) Lateral acceleration.

In order to investigate the relationship between sensitive long wavelength and train speed, a detailed study is given below. Train speed varies from a classic level of 250 km/h and 350 km/h to a potential level of 500 km/h.

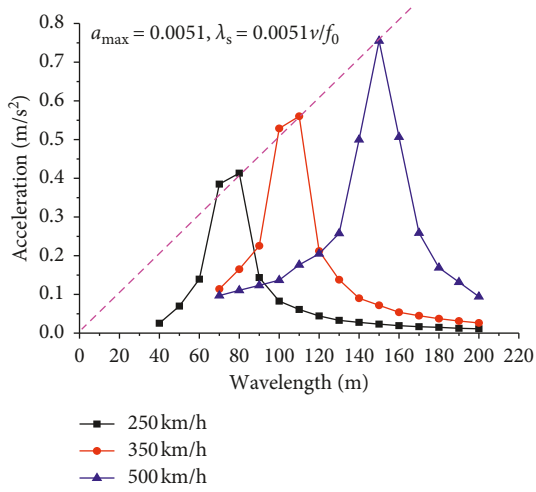

Figure 11: Vehicle vertical accelerations at different train speeds.

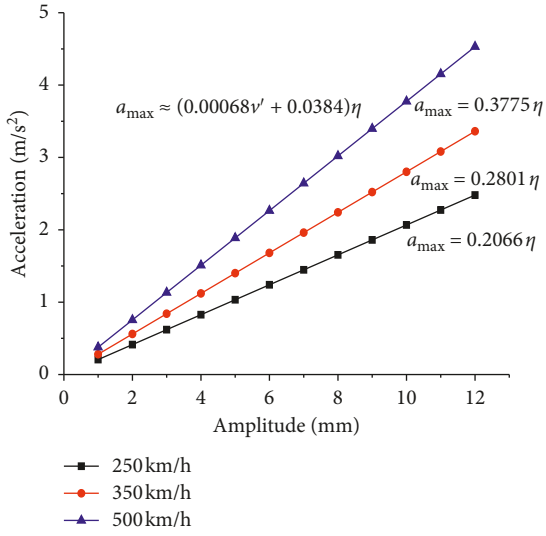

Figure 12: Vehicle vertical accelerations.

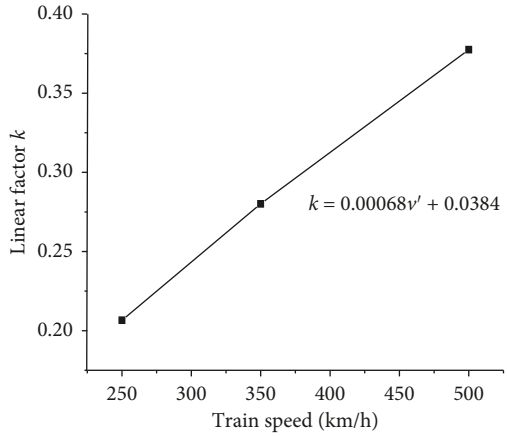

Figure 13: Linear factor at different train speeds.

Vertical vehicle accelerations are obtained to determine the sensitive long wavelengths at different train speeds using VTSDM as shown in Figure 11. The amplitude of track irregularities is fixed at 2 mm, and the wavelength varies from 40 to 200 m by the increment step 10 m. The maximum value of the vehicle acceleration a_{max} is excited

by the track irregularity with the sensitive long wavelength λ_s. It can be seen from Figure 11 that the sensitive long wavelengths at 250 km/h and 350 km/h are 80 m and 110 m, respectively.

Inferring from Figure 11, there is a linear relationship between the maximum acceleration a_{max} and the sensitive long wavelength λ_s, $a_{max} = 0.0051\lambda_s$. With further reference to equation (5), the relationship between a_{max} and train speed v' is established as follows:

$$a_{max} = 0.0051\frac{v}{f_0} = 0.0051\frac{v'/3.6}{0.92} \approx 0.0015v', \quad (6)$$

where the unit of v' is km/h.

3.2. Management Amplitude. After the sensitive long wavelength is determined, the dynamic effect of track irregularities with varying amplitudes is simulated based on VTSDM. The results are shown in Figure 12. It can be observed that the vertical accelerations under different train speeds increase linearly with the amplitude of track irregularities. The linear factor k is shown in Figure 13. There is also an approximate linear relationship between linear factor and train speed. Based on Figures 12 and 13, the relationship between vehicle acceleration, train speed, and track irregularities amplitude is described as follows:

$$a_{max} \approx (0.00068v' + 0.0384)\eta_{max}. \quad (7)$$

Note that the amplitude is corresponding to the sensitive long wavelength and also depends on the vehicle parameters. For a specific railway line, many trains might be on operation. The inspection of track irregularities should cover the maximum sensitive long wavelength. According to equations (6) and (7), the relationship between minimum sensitive long wavelength λ_{min} and maximum management amplitude η_{max} for the inspection and maintenance of track longitudinal-level irregularities are recommended as follows:

$$\begin{cases} \lambda_{min} > \lambda_s = \dfrac{v}{f_0} = \dfrac{v'/3.6}{0.92} = \dfrac{v'}{3.312}, \\ \eta_{max} \approx \dfrac{a_{max}}{0.00068v' + 0.0384} < \dfrac{[a]}{0.00068v' + 0.0384}, \end{cases} \quad (8)$$

where v' is the train speed and $[a]$ is the allowable value of vehicle vertical acceleration. $[a] = 1.0\,m/s^2$ is selected as a satisfactory value for ride comfort according to the China railway standard. To meet this standard, the minimum wavelength and the maximum amplitude are calculated and shown in Table 3.

3.3. Field Test and Validation. To validate the calculation results, some field tests have been carried out before the newly built high-speed railway lines were put into operation. During comprehensive and integrated tests, the inspection of track irregularities is an indispensable part. Sample data of measured track longitudinal-level irregularities are shown in Figure 14. The sensor position in field tests is shown in Figure 15. The measured vehicle vertical acceleration is shown in Figure 16(a). In order to compare with the filed test results, the sensor position in simulation is also placed as shown in Figure 15. The corresponding simulation result is shown in Figure 16(b). It can be inferred from Figure 16 that the peak values of measured and simulation results are $0.124\,m/s^2$ and $0.104\,m/s^2$ and the RMS values of measured and simulation results are $0.037\,m/s^2$ and $0.034\,m/s^2$, respectively. It indicates that simulation and measured results are in good agreement.

Meanwhile, frequency analysis of measured acceleration data has also been done. One measured vehicle acceleration is shown in Figure 17, and the frequency analysis result is shown in Figure 18. An obvious peak value is found around 1.0 Hz, which is the same as vertical natural frequency of

Table 3: Sensitive long wavelength and its corresponding management amplitude.

Train speed (km/h)	Wavelength (m)	Amplitude (mm)
250	80	5
350	110	4
500	150	3

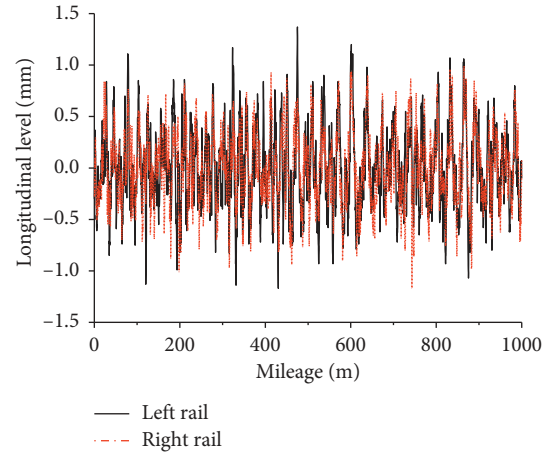

Figure 14: Measured track longitudinal-level irregularities.

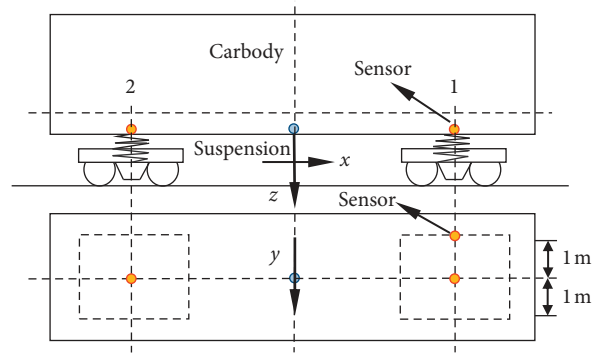

Figure 15: Sensor position.

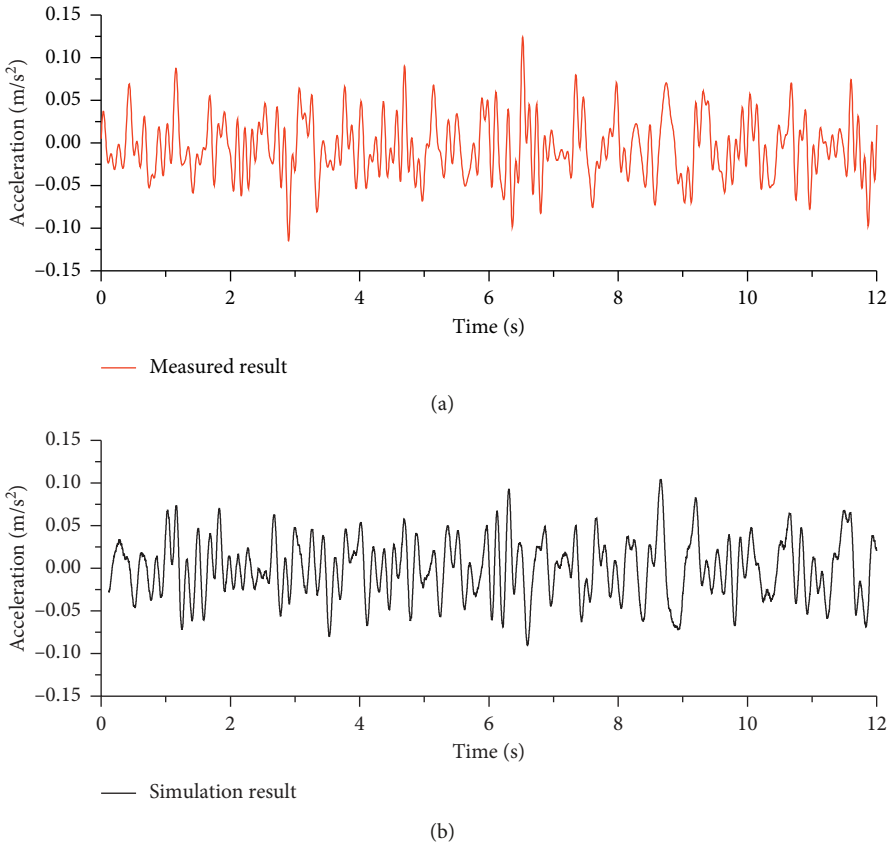

Figure 16: Vehicle accelerations. (a) Measured result. (b) Simulation result.

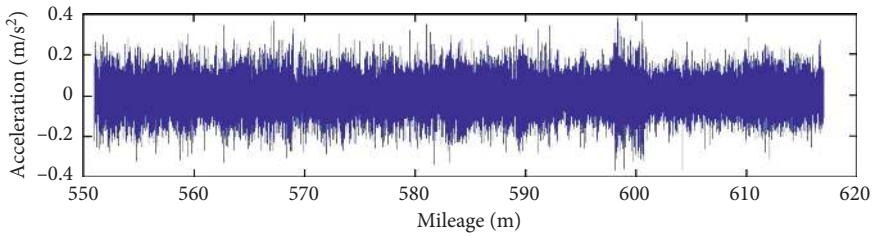

Figure 17: Signal sample of vehicle vertical acceleration.

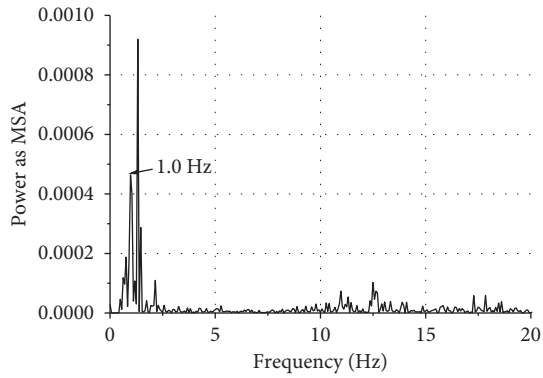

Figure 18: PSD calculation sample.

Table 4: Sensitive long wavelength of longitudinal-level irregularities for different trains.

Speed (km/h)	Sensitive long wavelength (m)		
	CIT001	CRH2	CRH380
250	50	60	80
350	80	90	120

carbody. The natural frequency of carbody is used to determine the maximum sensitive wavelength of track irregularities.

After processing the field test data through Fourier transform, the sensitive long wavelengths for three typical types of track geometry car are obtained. Each train runs on the track at the speed of 250 km/h and 350 km/h. The results are shown in Table 4.

CRH series are the main types of passenger trains used in Chinese high-speed railway. CIT refers to high-speed Comprehensive Inspection Train. CIT001 is officially named as Zero Comprehensive Inspection Train. It can be observed from Table 4 that there are some differences between them, especially between CRH380 and CIT001. The sensitive long wavelength for CRH380 at 350 km/h is around 120 m, while it is 80 m for CIT001. Further research is carried out in China to develop new inspection trains for covering sensitive long wavelength which is up to 150 m.

For CRH380, at train speed 250 km/h, the sensitive long wavelengths of longitudinal-level irregularities from calculation and field tests are both 80 m. At train speed 350 km/h, the sensitive long wavelengths are 110 m and 120 m, respectively. A good agreement between simulation results and field test results is observed.

4. Conclusions

The dynamic responses of high-speed trains' operating on slab tracks are investigated based on VTSDM. Track irregularities are the only excitation source. One case study is presented to show the methodology of determining the sensitive long wavelengths and management amplitude under varying train speeds. The conclusions drawn from this study are presented as follows:

(a) The acceleration of the carbody selected as the indicator of ride comfort has been proved to have a significant relationship with long-wavelength track irregularities. For track longitudinal-level irregularities, the sensitive long wavelengths depend on the vertical natural frequencies of vehicles and train speeds.

(b) Within the speed ranging from 250 km/h to 500 km/h, there is a clear linear relationship between the acceleration of carbody and train speeds and also between the acceleration and track irregularities amplitude. Based on the linear relationship, one regression formula was proposed to determine the sensitive long wavelength and management amplitude of track longitudinal-level irregularities.

(c) Field tests of CRH380 were used to validate the proposed formula. There is a good agreement between simulation and test results.

Data Availability

We declare that all data are authentic and available. The simulation and field test data used to support the findings of this study are included within the article.

Conflicts of Interest

The authors declare that there are no conflicts of interest.

Acknowledgments

The authors wish to appreciate the financial support provided by the National Natural Science Foundation of China (51678047); Key Laboratory of Roads and Railway Engineering Safety Control (Shijiazhuang Tiedao University), Ministry of Education (STKF201716); and Research and Development Program of China Railway Corporation (2017G011).

References

[1] D. P. Connolly, G. P. Marecki, G. Kouroussis, I. Thalassinakis, and P. K. Woodward, "The growth of railway ground vibration problems-a review," *Science of the Total Environment*, vol. 568, pp. 1276–1282, 2016.

[2] G. Kouroussis, D. P. Connolly, G. Alexandrou, and K. Vogiatzis, "The effect of railway local irregularities on ground vibration," *Transportation Research Part D: Transport and Environment*, vol. 39, pp. 17–30, 2015.

[3] K. E. Vogiatzis and G. Kouroussis, "Environmental groundborne noise and vibration from urban light rail transportation during construction and operation," *Current Pollution Reports*, vol. 3, no. 2, pp. 162–173, 2017.

[4] A. Klockner, A. Knoblach, and A. Heckmann, "How to shape noise spectra for continuous system simulation," *Mathematical and Computer Modelling of Dynamical Systems*, vol. 23, no. 3, pp. 284–300, 2017.

[5] G. Kouroussis, H. P. Mouzakis, and K. E. Vogiatzis, "Structural impact response for assessing railway vibration induced on buildings," *Mechanics and Industry*, vol. 18, no. 7, p. 703, 2017.

[6] C. F. Hung and W. L. Hsu, "Influence of long-wavelength track irregularities on the motion of a high-speed train," *Vehicle System Dynamics*, vol. 56, no. 1, pp. 95–112, 2018.

[7] G. Kouroussis, D. P. Connolly, K. Vogiatzis, and O. Verlinden, "Modelling the environmental effects of railway vibrations from different types of rolling stock: a numerical study," *Shock and Vibration*, vol. 2015, Article ID 142807, 15 pages, 2015.

[8] X. Yang, S. Gu, S. Zhou, J. Yang, Y. Zhou, and S. Lian, "Effect of track irregularity on the dynamic response of a slab track under a high-speed train based on the composite track element method," *Applied Acoustics*, vol. 99, pp. 72–84, 2015.

[9] L. Xu, W. Zhai, J. Gao, M. Meacci, and X. Chen, "On effects of track random irregularities on random vibrations of vehicle-

track interactions," *Probabilistic Engineering Mechanics*, vol. 50, pp. 25–35, 2017.

[10] L. Ling, Y. Q. Deng, Q. H. Guan, and X. S. Jin, "Effect of track irregularities on the dynamic behavior of a tram vehicle," *Advances in Vehicle Engineering*, vol. 3, no. 1, pp. 29–39, 2017.

[11] J. Sadeghi, A. Khajehdezfuly, M. Esmaeili, and D. Poorveis, "Investigation of rail irregularity effects on wheel/rail dynamic force in slab track: comparison of two and three dimensional models," *Journal of Sound and Vibration*, vol. 374, pp. 228–244, 2016.

[12] A. Nokhbatolfoghahai, M. A. Noorian, and H. Haddadpour, "Dynamic response of tank trains to random track irregularities," *Meccanica*, vol. 53, no. 10, pp. 2687–2703, 2018.

[13] L. Xu, W. Zhai, and Z. Chen, "On use of characteristic wavelengths of track irregularities to predict track portions with deteriorated wheel/rail forces," *Mechanical Systems and Signal Processing*, vol. 104, pp. 264–278, 2018.

[14] P. Czop, K. Mendrok, and T. Uhl, "Application of inverse linear parametric models in the identification of rail track irregularities," *Archive of Applied Mechanics*, vol. 81, no. 11, pp. 1541–1554, 2011.

[15] H. Fujimoto, K. Tanifuji, and M. Miyamoto, "Influence of track gauge variation on rail vehicle dynamics (an examination based on comparison between data from a test train running on track with irregularity artificially set and numerical simulation)," *Proceedings of the Institution of Mechanical Engineers, Part F: Journal of Rail and Rapid Transit*, vol. 214, no. 4, pp. 223–230, 2000.

[16] P. Gullers, L. Andersson, and R. Lunden, "High-frequency vertical wheel-rail contact forces - field measurements and influence of track irregularities," *Wear*, vol. 265, no. 9-10, pp. 1472–1478, 2008.

[17] T. Karis, M. Berg, S. Stichel, M. Li, D. Thomas, and B. Dirks, "Correlation of track irregularities and vehicle responses based on measured data," *Vehicle System Dynamics*, vol. 56, no. 6, pp. 967–981, 2018.

[18] A. Haigermoser, B. Luber, J. Rauh, and G. Gräfe, "Road and track irregularities: measurement, assessment and simulation," *Vehicle System Dynamics*, vol. 53, no. 7, pp. 878–957, 2015.

[19] Q. Q. Li, Z. P. Chen, Q. W. Hu, and L. Zhang, "Laser-aided INS and odometer navigation system for subway track irregularity measurement," *Journal of Surveying Engineering*, vol. 143, no. 4, 2017.

[20] S. Iwnicki, D. Thompson, M. Berg, C. Cole, Y. Boronenko, and E. Andersson, *Handbook of Railway Vehicle Dynamics*, CRC Press, Boca Raton, FL, USA, 2006.